X-ray magnetic circular dichroism study of the magnetic anisotropy on $TbMnO_3$

V. Cuartero[1*], S. Lafuerza[1], G. Subías[2], J. García[2], E. Schierle[3], J. Blasco[2], J. Herrero-Albillos[2,4]

[1]*ESRF-The European Synchrotron, 71, Avenue des Martyrs, Grenoble (France)*
[2]*Instituto de Ciencia de Materiales de Aragón, Departamento de Física de la Materia Condensada, CSIC-Universidad de Zaragoza, C/ Pedro Cerbuna 12, 50009 Zaragoza (Spain)*
[3]*Helmholtz Zentrum Berlin Mat & Energie, D-12489 Berlin, (Germany)*
[4] *Centro Universitario de la Defensa, Ctra. De Huesca s/n, 50090 Zaragoza (Spain)*

**corresponding author: cuartero@esrf.fr*
PACS: 75.25.-j, 75.30.Gw, 75.47.Lx, 75.85.+t

Abstract. The magnetic anisotropy of $TbMnO_3$ was explored by means of polarized x-ray absorption spectroscopy and x-ray circular magnetic dichroism (XMCD) measurements at the Mn $L_{2,3}$ and Tb $M_{4,5}$ edges, as a function of temperature and magnetic field intensity. The selective magnetometry measurements were compared with the macroscopic magnetic properties on single crystals. XMCD measurements at the Tb $M_{4,5}$-edge as a function of the magnetic field reproduces quite well the macroscopic magnetic anisotropy at low temperatures with the Tb moments staying confined along their Ising axis within the *ab* plane while a weak XMCD signal is observed at the Mn $L_{2,3}$-edge. These results point out that Tb^{3+} single ion anisotropy is the only responsible for the magnetic anisotropy on this multiferroic compound at high magnetic fields. Moreover, we found Mn $L_{2,3}$ XMCD measurements show that the cycloidal antiferromagnetic order is almost unaffected by the applied magnetic field. at low temperatures under an applied magnetic field. Therefore, we discuss that this strong Ising nature of Tb^{3+} ions, through a magneto-crystalline coupling, mediated by the oxygen atoms, must play an important role on the field-induced electric polarization flop and therefore on the magneto-electric coupling on $TbMnO_3$.

I. Introduction

Rare earth (RE)-transition metal (TM) oxides show a great variety of intriguing phenomena originating from the coupling between the two spin subsystems[1]. Multiferroicity and magnetoelectric coupling are among them[2,3]. However, the combination of a magnetic ordered ground state together with ferroelectricity (FE) is not trivial[4,2] and many attempts have been made in the last years to explain the occurrence of these two phenomena in the same phase. In the case of type II multiferroics[5], where FE is driven by a non-collinear magnetic ordering of the TM sublattice, the inversion symmetry breaking is due to the anisotropic exchange interaction also known as Dzyaloshinskii-Moriya interaction[6], which promotes a net electric polarization. The electric polarization is then given by $\vec{P} \sim \lambda_{so} \vec{r}_{ij} \times \left(\vec{S}_i \times \vec{S}_j\right)$, where $\vec{S}_{i,j}$ refers to the magnetic moment of two first neighbours *i*, *j*,

separated by a distance $\vec{r}_{ij}$ and λ_{SO} is the spin-orbit coupling constant, from which it is inferred that electric and magnetic properties are completely coupled.

This is the case for $TbMnO_3$, an orthorhombic perovskite (space group *Pbnm*) where a sinusoidal-wave-type ordering of the Mn^{3+} spins along the **b** axis order antiferromagnetically along the **c** axis (so-called A_y-type order). This type of spin order has an onset at $T_{N,Mn} \approx 41$ K. Upon cooling in zero fields a second magnetic transition into a spiral phase occurs at about 28 K with the cycloidal spin structure oriented in the *bc* plane, and consequently the onset of spontaneous electric polarization parallel to the **c** axis. The antiferromagnetic ordering of Tb spins occurs at $T_{N,Tb} \approx 7$ K[7,8]. However, several spectroscopy experiments point out that the magnetic coupling between Mn and Tb that is present even above $T_{N,Tb}$, play the main role on the appearance of multiferroicity and magnetoelectric coupling.[9-14] Moreover, in an applied magnetic field a more complex behavior is found and magnetic fields can control the direction of electric polarization[15]. Results showed a spin-flop transition of Mn moments, contained on the *bc* plane at zero field (and **P**//**c**), into a configuration lying on the *ab* plane for **H**//**a** or **H**//**b** (then **P**//**a**)[8]. Besides that, the macroscopic magnetic response of $TbMnO_3$ is highly anisotropic depending on the direction of the applied external magnetic field with respect to the crystallographic axis[16], **a** being the easy magnetization axis and **c** the hard magnetic axis. For instance, at 9 T and 5 K, the values of the magnetization are M_a=6.5 μ_B/fu, M_b=3.7 μ_B/fu and M_c=1.1 μ_B/fu, while 4 μ_B per ion are expected for a saturated Mn^{3+} lattice ($3d^4$, $^5D_0$ ground state) and 9 μ_B is the theoretical magnetic moment per ion for a fully polarized Tb^{3+} sublattice ($4f^8$, $^7F_6$ ground state). In addition, below 7 K, the application of an external magnetic field leads to metamagnetic transitions of the Tb^{3+} moments. In particular, a field parallel to the *b* axis induces a commensurate long-range ordering of Tb of type *CxFy*.[17]

In order to disentangle the magnetic contributions responsible for the macroscopic magnetic anisotropic behavior under applied magnetic fields on $TbMnO_3$, we have investigated the differentiated role of Mn and Tb ions by soft x-ray absorption spectroscopy (XAS) and x-ray magnetic circular dichroism (XMCD) at Tb $M_{4,5}$ and Mn $L_{2,3}$ edges, as a function of temperature and the intensity and direction of the applied magnetic field. We recall here that $TbMnO_3$ is a strong insulating sample at low temperatures suffering from sample charging, which limits the applicability of the most practiced total electron yield (TEY) detection method. Therefore, we have also performed XMCD measurements in either total fluorescence yield (TFY) or reflection modes[18]. Moreover, as the studied samples are thick single crystals, XAS spectra measured in TFY must be corrected for self-absorption, as will be addressed here. From this thorough study, it can be concluded that Tb magnetism dominates the observed strong magnetocrystalline anisotropy in $TbMnO_3$ (Mn contributions are at least a factor of 6 smaller). Consequently the different field-dependent behavior of the magnetization along the three crystallographic axes reflects the Ising nature of the Tb^{3+} moments that is brought in by the combination of spin-orbit coupling with the low-symmetry environment of the Tb sites in the *Pbnm* structure. Moreover, this strong Ising character of Tb in $TbMnO_3$ is also playing an important role on the electric polarization flop from **c** to **a** axis under applied magnetic fields.

II. Experimental Details

$TbMnO_3$ polycrystalline samples were prepared by the ceramic method: stoichiometric amounts of Tb_4O_7 and $MnCO_3$ were mixed, ground and heated up at 1000º C during 12 h as a first step. The resulting powder was pressed into pellets and sintered at 1200º C during 24 h in air. As a last step, the samples were repressed into pellets and sintered at 1400º C under Ar atmosphere during 48 h. X-ray diffraction patterns were collected with a Rigaku D/max-B diffractometer, with a copper rotating anode and a graphite monochromator in order to select the Cu Kα wavelength (λ = 1.5418 Å). The patterns were in agreement with a single phase orthorhombic perovskite, space group *Pbnm* and the samples were then used as the feed and seed rods for the single crystal growth. $TbMnO_3$ single crystals were grown by the floating zone method using a homemade furnace with two semielliptical mirrors.[19] The feed and seed rods were rotating in opposite directions at ±20 rpm and the growth speed was 8 mm/h. The growth was carried out under Ar atmosphere and a boule of 7 cm was obtained. Three crystals were cut so that their faces were perpendicular to **a**, **b** and **c** crystallographic axis.

The macroscopic magnetization measurements as a function of temperature and applied magnetic field up to 60 kOe were performed with commercial PPMS from Quantum Design using the Vibrating Sample Magnetometry (VSM) configuration.[17]

Soft x-ray spectroscopy measurements were performed at the high-field diffractometer of the UE46-PGM1 beamline at BESSY-II synchrotron (Helmholtz-Zentrum, Berlin, Germany). XAS and XMCD measurements at the Tb $M_{4,5}$ edges (from 1220 eV to 1290 eV) and the Mn $L_{2,3}$ edges (from 635 eV to 665 eV) were carried out from 100 K down to 5 K with an applied magnetic field up to 6 T oriented along the three different crystallographic axis. XMCD spectra were obtained as the difference between two absorption spectra measured with opposite x-ray beam helicity (right μ^+ and left μ^- circular polarizations, XMCD= μ^+-μ^-) and a fixed magnetic field direction. The dichroic signals are normalized to the maximum intensity of the averaged XAS spectrum obtained by merging (μ^++μ^-)/2 and will be represented as a percentage of the XAS signal. The helicity of the x-ray beam was changed by reversing the phase of the helical undulator and the degree of circular polarization was 90%. A PGM plane grating monochromator was used and the primary slits were opened in order to find the best compromise between photon flux and energy resolution (1.2 eV).

Three detection modes were used to carry out the spectroscopic measurements at the Tb $M_{4,5}$ edges under ultra-high vacuum conditions: TFY, reflection and TEY. Here reflectivity and TFY measurements will be presented, more sensitive to the bulk properties of the system. The corresponding geometrical configurations are plotted on figure 1. XMCD measurements in reflection geometry (R-XMCD) were performed in a cleaved single crystal with [001] surface normal in order to get a clean surface (fig. 1(a)). X-rays impinged the sample at a fixed grazing incidence angle θ ~ 6-8° and the magnetic field was applied for either **H**//**a** or **H**//**b** allowing magnetization of the sample parallel to its surface. The outgoing photons were collected by a photodiode. Simultaneous TFY and TEY detection modes were used for **H**//**c** configuration in a polished single crystal with [001] surface normal covered

with a graphite mesh to ensure electrical conductivity at low temperatures. A photodiode was placed at about 80° with respect to the incident beam as can be seen on figure 1 (b). The self-absorption effects and their correction will be discussed in the next section. At the Mn $L_{2,3}$ edges, only TEY detection was used on a polished single crystal with [010] surface normal covered with a graphite mesh (fig. 1(c)).

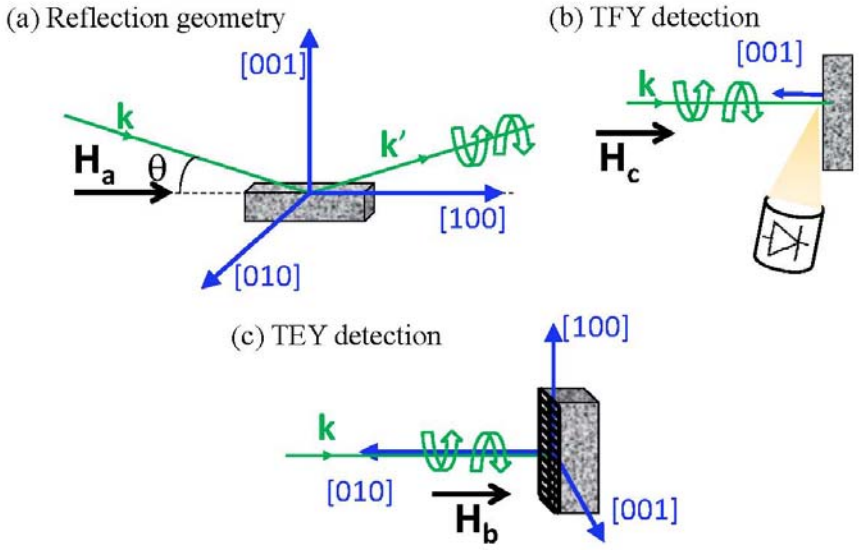

Figure 1. Configurations of the detection modes used at the experiment. (a) Reflection geometry, where there is a small angle (≤ 8°) between the direction of the magnetic field and the photon's propagation vector. (b) TFY, where the fluorescence emitted photons are detected by a photodiode placed at ~80° with respect to the incoming photons to reduce Compton scattering. (c) TEY, where the electron scattering cascade following the Auger decay is measured via the sample drain current.

III. Results and Discussion

A. XMCD at the Tb $M_{4,5}$ edge

The Tb $M_{4,5}$-edge μ^+ and μ^- spectra measured in reflection geometry with an applied magnetic field **H**//**a** of 5 T at 5 K are shown in fig. 2 as well as the XMCD signals with the applied magnetic field parallel to both [100] and [010] crystallographic directions, following the experimental set-up described in figure 1(a). The Tb 3*d*-4*f* absorption spectrum is characterized by two structures (M_5 and M_4) well separated in energy by the strong spin-orbit interaction. The dichroism is very strong as expected for a rare earth atom having a high spin magnetic moment. The high XMCD intensity at the M_5 edge compared to the low intensity at the M_4 edge indicates a strong contribution from the orbital moment of the Tb ion.[20]

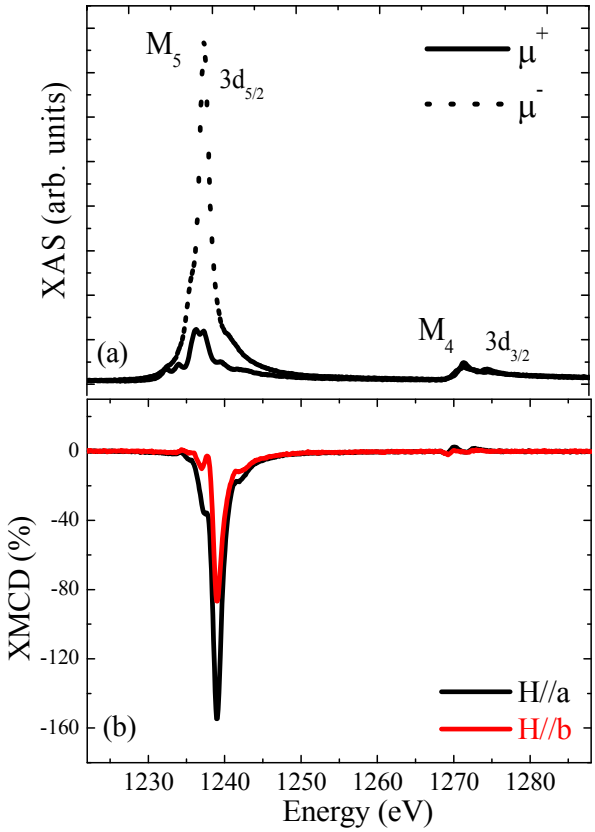

Figure 2. (a) XAS spectra taken at the $M_{4,5}$ edges of Tb with right (μ^+) and left (μ^-) circular polarization for **H**//**a** configuration at T=5 K and H=5 T. (b) Normalized XMCD spectra with 5 T magnetic field applied along the [100] and [010] crystallographic directions at T=5 K.

The overall spectral line shape of the XMCD signal is very similar for the two crystallographic directions and resembles other XMCD spectra measured in different terbium systems at the Tb $M_{4,5}$ edge.[21-23] However, the amplitude of the dichroism is considerably different: 160% (**H**//**a**) and 85% (**H**//**b**).

For the **H**//**c** configuration, we used TFY detection as described in fig. 1(b). Under this geometry, self-absorption effects become important due to the longer penetration depth of x-rays. The self-absorption effects can be corrected by taking into account geometrical factors in such a way that the experimental fluorescence absorption spectra μ_F results into[24]

$$\mu_F(E) = \frac{\left(\frac{\Omega}{4\pi}\right)\varepsilon_f \mu(E)}{\mu_T(E) + \mu_T(E_f)\frac{\sin\theta}{\sin\varphi}} \qquad (1)$$

$\mu_T(E)$ being the total absorption coefficient including contributions from the edge of interest and from other edges of all atoms in the compound ($\mu(E) + \mu_{bkg}(E)$) and $\mu_T(E_F)$ the total absorption coefficient at the energy of the fluorescence photons E_F. θ and φ are the angles between the sample surface and the direction of the incoming and the detected fluorescence photons, respectively. Finally, $\Omega/4\pi$ is the solid angle covered by the detector and ε_f is the fluorescence yield of the absorber atom.

In this case, $\mu_T(E)$ can be approximated to $\mu_T(E) = \mu(E) + k$, where k is constant since the energy range at the Tb $M_{4,5}$-edges is small. Taking into account equation (1) and grouping all the constant factors, we can rewrite the absorption coefficient without self-absorption effects as follows

$$\mu(E) = \frac{C_1 \mu_F(E)}{C_2 - \mu_F(E)} = \mu_{TEY}(E) - \mu_{bkg}(E) \qquad (2)$$

Therefore, TEY-detected μ^+ and μ^- experimental spectra (background subtracted) were fitted to the corresponding $\mu_F(E)$ measurement to obtain C_1 and C_2 fitting constants. To do so, TEY and FY spectra were measured simultaneously. Then, equation (2) was applied to FY spectra to finally obtain the absorption coefficient $\mu(E)$ free of self-absorption effects. The estimated error of this procedure is about 10% which is inside the total estimated experimental uncertainly. The comparison between μ_{TEY}, μ_F and the final μ obtained after the self-absorption correction can be seen on figure 3. The ratio between M_5 and M_4 edges is satisfactorily corrected and the line shape changes accordingly.

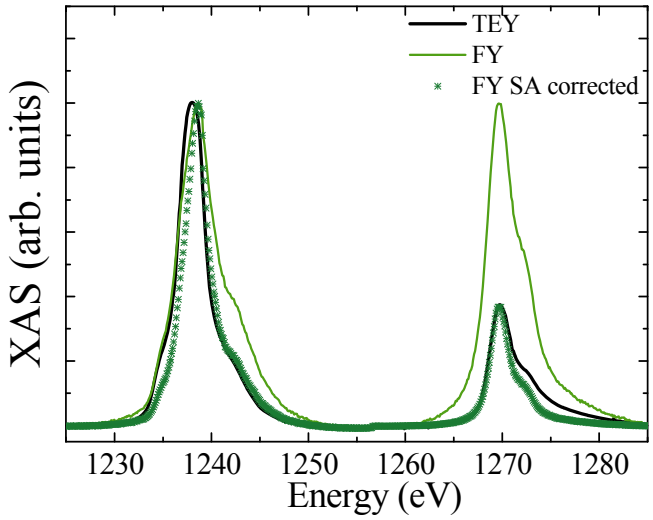

Figure 3. XAS spectra normalized to the maximum of M_5 edge measured in TEY, in FY and self-absorption (SA) corrected (points) at 5 K without applied magnetic field.

After the self-absorption correction, the normalized Tb $M_{4,5}$ edge XAS and XMCD spectra at 5 K with the magnetic field of 5 T applied along the crystallographic *c* axis are shown in fig. 4. The amplitude of the dichroic signal is 28%, much smaller than for **H**//**a** and **H**//**b** configurations. We note here that the maximum values of the XMCD signals along the three crystallographic directions are strongly anisotropic and proportional to the magnetization M_a, M_b and M_c, respectively at T=5 K and H=5 T[16].

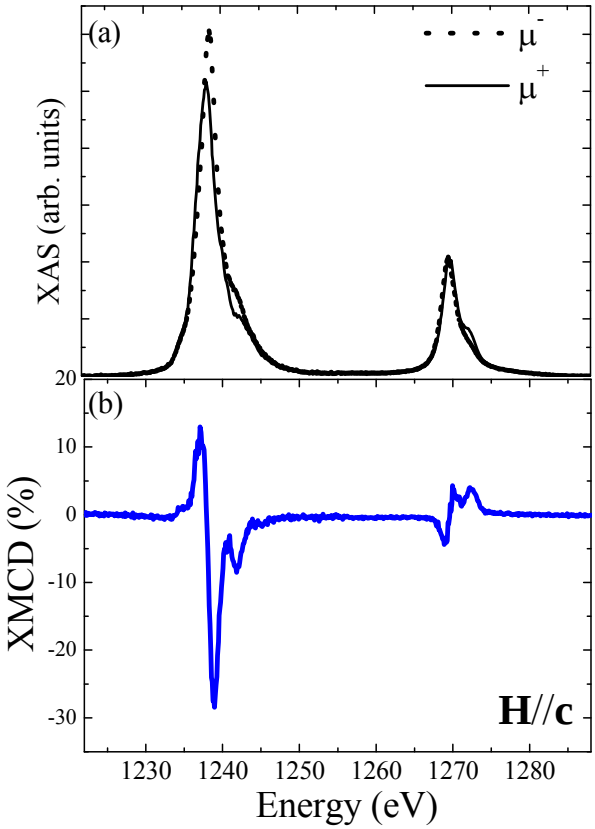

Figure 4. (a) Self-absorption corrected XAS spectra taken at the $M_{4,5}$ edges of Tb with right (μ^+) and left (μ^-) circular polarization for **H**//**c** configuration at T=5 K and H=5 T. (b) Normalized XMCD spectra with 5 T magnetic field applied along the [001] crystallographic direction at T=5 K.

To track the evolution of Tb contribution to the magnetization anisotropy, we measured the Tb $M_{4,5}$ edge XMCD signals as a function of magnetic field at T=5 K, below $T_{N,Tb}$. Figure 5 shows the integrated XMCD signal at the Tb M_5 edge normalized by the maximum of the corresponding averaged XAS spectrum for the complete set of values of the applied magnetic field (0-5 T) along the three crystallographic *a*, *b* and *c* axes. In fig. 5 it is also shown the field dependence macroscopic magnetization measurements at T=5 K, which indicate a strong anisotropy with the local moments almost confined in the *ab* plane but also show anisotropic magnetization within this *ab* plane. Indeed, the change on the evolution of the magnetization slope around 4.5 T along **b** axis is well reproduced by the XMCD integrated signal, within the error bars. At 5 K, Tb moments exhibit an incommensurate antiferromagnetic order at zero fields so this step in the slope for H||b at 4.5-5 T corresponds well with the metamagnetic transition observed in the results previously reported.[16,17] In addition, the saturation trend along **a** axis above 3T is also followed by the integrated signal obtained for **H**//**a**. For **H**//**c**, magnetization increases almost linearly with increasing field, while staying far smaller than M_{ab}. This field behavior is also well reproduced by the XMCD integrated signal obtained for **H**//**c**. Then, the strong magnetic anisotropy in $TbMnO_3$ is mostly related to the Tb-sublattice magnetism, with Tb magnetic moments mainly contained within the *ab* plane.

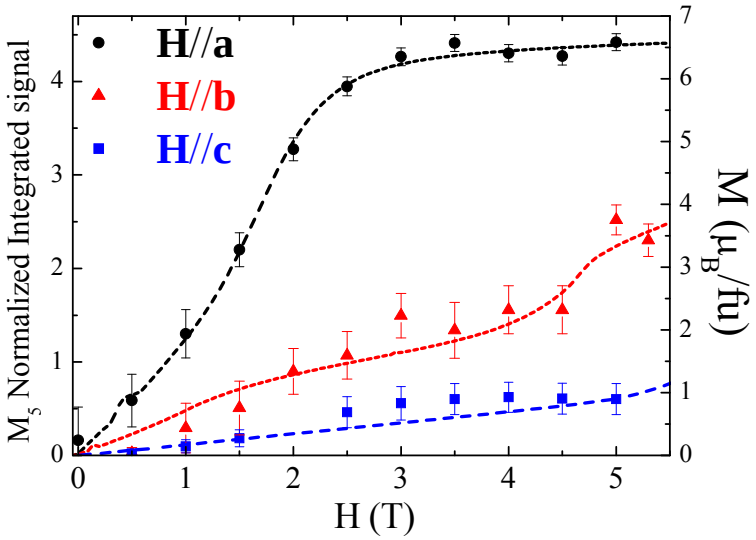

Figure 5. Macroscopic magnetization (dotted lines) as a function of external field (taken at T=5 K) along the three crystallographic axes of the $TbMnO_3$ single crystal compared to the normalized Tb M_5 edge integrated XMCD signal (solid symbols).

Aiming at elucidating the underlying physics the experimental spectra were fitted with theoretical ones. The calculation of absorption and dichroic spectra were based on atomic multiplets performed with CTM4XAS program[25]. In order to simulate the Tb XAS spectra, we considered the Tb^{3+} single ion for an initial $3d^{10}4f^{8}$ and final $3d^{9}4f^{9}$ states and we included the crystal field point symmetry by branching from SO_3 symmetry to O_h, then lowering the symmetry to D_{4h} and finally to C_{4h}, according to the Butler branching rules for the symmetry elements.[26] The relevant atomic Hartree-Fock values of the electrostatic integrals (F^k) and exchange parameters (G^k) calculated with Cowan's code[27] were scaled down to 80% and 99% respectively. The comparison between the experimental spectra obtained from the merge of the XAS spectra along the three crystallographic directions and the theoretical (isotropic average) calculation is shown in figure 6. Both XAS spectra are normalized to the maximum of the M_5 edge.

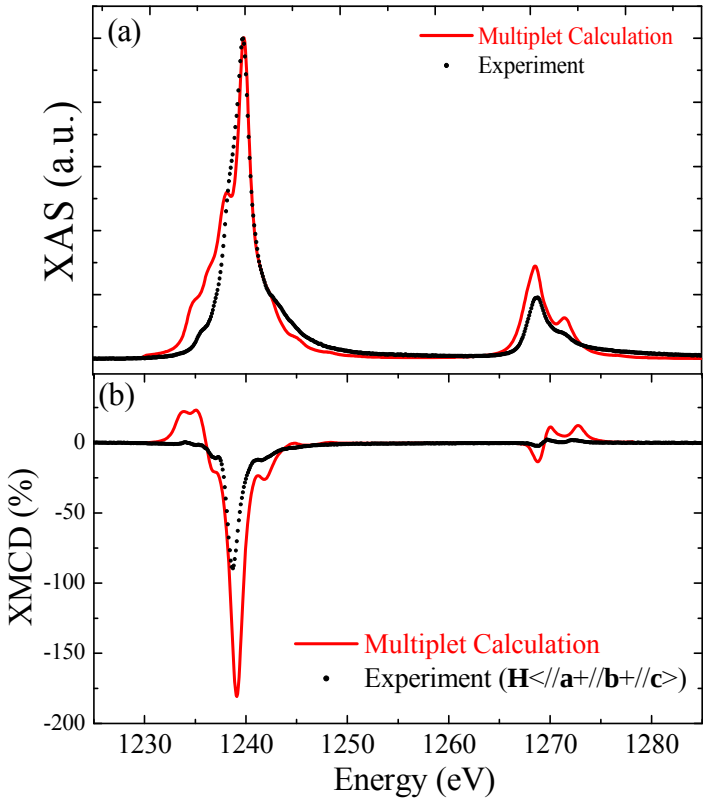

Figure 6. Comparison of experimental (dots) average XAS spectra (a) and average XMCD spectra (b) merged along the 3 crystallographic directions (**H**<//**a**+//**b**+//**c**>) taken on $TbMnO_3$ cleaved single crystals with the results of multiplet calculations (solid lines). For experiment, temperature and external magnetic field were 5 K and 5 T, respectively.

The agreement of the calculations with the experimental data is reasonable and reproduces the main features of the spectra. Minor differences are found in the line shape and can be attributed to the fact that in reflection geometry, the shape of the XAS and XMCD spectra depends not only on absorption but also on dispersion. However, the intensity of the experimental XMCD signal is reduced with respect to the atomic multiplet calculation. To determine the value of the Tb magnetic moment, we exploited the calculated spectra to check first the validity of the application of the sum rules[28,29] to this system. In their application we followed ref. 28, considering that the dipolar transition rule for Tb^{3+} ($4f^{8}$) at $M_{4,5}$ edges gives c=2 (*d* initial state) and l=3 (*f* final state). Then, the expectation values of the projection of the orbital and spin moments are,

$$< Lz >= \frac{q \cdot (14 - n)}{r}$$

$$< Sz >= \frac{(5p - 3q) \cdot (14 - n)}{4r} - 3 < Tz >$$

where $q = \int_{M4+M5} dw(\mu^{+} - \mu^{-})$, $p = \int_{M5} dw(\mu^{+} - \mu^{-})$ and $r = \int_{M4+M5} dw(\mu^{+} + \mu^{-})/2$, while <Tz> is the expectation value of the intra-atomic magnetic dipole operator. Here it is considered for

Tb^{3+} ion the atomic value T_z/S_z=-0.081, as it has been previously calculated.[30] The Lz and Sz values derived from the sum rules applied to the calculated spectra are -3.3 and -2.6, respectively, being the Tb total magnetic moment $m_z=-(2S_z+L_z)=8.6\pm0.2$ μ_B. These values agree within 10% with the expected ones for a free Tb^{3+} ($4f^8$) with a Hund's rule ground state J=6, namely L=3, S=3 and theoretical saturation moment of 9 μ_B. We then applied the sum rules to the experimental spectra merged along the three crystallographic directions (<**a**+**b**+**c**>) under an applied magnetic field of 5 T. The expectation values for Lz and Sz are -1.6 and -2.5 respectively, giving a Tb magnetic moment of 5.8 μ_B. The experimental Tb magnetic moment found at 5T is much smaller than the single ion saturation value but it is close to the merged value of the magnetic moment along **a** and **b** directions (5.6 μ_B), which corresponds to the plane where Tb magnetic moments are mostly confined.

This magnetic behavior is in agreement with the strong Ising character of Tb^{3+} and the four-sublattice model proposed for the antiferromagnetic state below $T_{N,Tb}$ in various perovskite compounds.[31-32] Tb^{3+} ($4f^8$) is a non-Kramers ion being $^7F_6$ the lowest lying free-ion term, but in $TbMnO_3$, similarly to $TbAlO_3$[33], the crystal field of Tb Wyckoff position *4c* with point symmetry *Cs* (subgroup of C_{4h}), splits this ground state multiplet into 2J+1=13 singlets. As expected from the energy balance between the crystal field splitting (tenths of meV) and the Zeeman energy splitting at 5 T (meV), the lowest crystal-field level is a quasi-doublet that can be approximated by a linear combination of "pure" |6, ±6> states, corresponding to the magnetic moment of a free-Tb^{3+} ion, i.e. 9 μ_B[33]. Besides, the large crystalline anisotropy of Tb^{3+} fixes the magnetic moments of the two inequivalent Tb sites in *Pbnm*, related by a mirror reflection in the *ac* plane, along their respective Ising axes (the anisotropy axis), resulting in noncollinear ordered arrangements within the *ab* plane[31-32]. On the other hand, at zero external fields and below $T_{N,Tb}$ Tb sublattice shows an incommensurate antiferromagnetic order,[8] while for $T_{N,Tb}<T<T_{FE}$=27K both Mn and Tb orderings have been shown to be coupled with the same wave vector[9-14], whereas for $T>T_{FE}$=27K, Tb is in the paramagnetic state. Therefore, in zero field and $T > T_{FE}$, the magnetic moments α_1, α_2 and β_1, β_2 of the four Tb sites in the orthorhombic cell are disordered along the two Ising directions -ϕ_0 and +ϕ_0 , from **a** axis, respectively, with no net magnetization (Fig. 7a). The application of a magnetic field parallel to the **a**- or **b**-axis aligns the Tb paramagnetic moments in the field direction but along the Ising axes of the two inequivalent Tb sites, resulting into pairs of aligned magnetic moments at an angle ϕ_0 from **a**-axis (Fig. 7b) or **b**-axis (Fig 7d). However, below $T_{N,Tb}$ the orientation of the Tb moments following the applied field competes with the antiferromagnetic order and consequently metamagnetic changes are manifested as a step behavior in the M(H) curves. Then, at $T<T_{N,Tb}$ when **H**//**a,** the flipping of the magnetic moments occurs at low fields about 1.5 T, whereas if **H**//**b**, two discontinuities are observed and a canted antiferromagnetic order is likely to be stable between 2 T and 4.5 T. At a first approximation, we can consider the simple two-steps model for the flipping of Tb moments along *b*, as for related perovskites. At $\mathbf{H_b}$~2 T, the magnetic moment of just one of the two inequivalent Tb sites is aligned along its Ising axis in the field direction (Fig. 7c) while the second one is aligned at $\mathbf{H_b}$~4.5 T (Fig. 7d) [34]. Finally, we would like to note that the magnitude of the Tb magnetic moment and the canted angle ϕ_0 deduced from the

experimental magnetization values, along **a** and **b** axes in high magnetic fields (> 5T) and below T_N(Tb), are 8.2 μ_B and 34º, respectively[17], which justifies that the ground-state quasi-doublet (|6, 6> ± |6, -6>/√2) does not couple with higher crystal field levels at low temperatures.

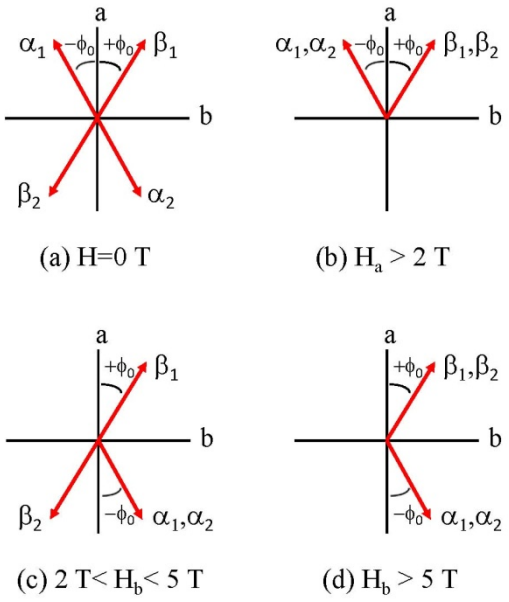

Figure 7. Tb magnetic moment configuration projected in the *ab* plane in $TbMnO_3$ at low temperatures (T=5 K). (a) H=0; (b) H>2.5 T applied along the *a*-axis; (c) 2 T<H<5 T applied along the *b*-axis and (d) H>5 T applied along the *b*-axis.

B. XMCD at the Mn $L_{2,3}$ edge

Attention is now paid to the Mn magnetic contribution. Figure 8 shows the XMCD signal using TEY as detection mode for **H**//**b** as well as XAS spectra taken at the Mn $L_{2,3}$ edges with both helicities for the $TbMnO_3$ single crystal with [010] surface normal. Temperature and magnetic field were 5 K and 5 T, respectively.

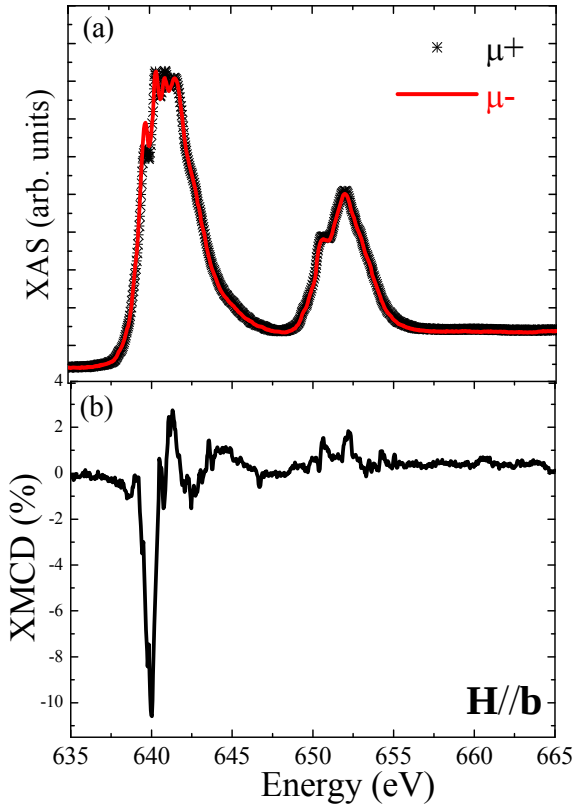

Figure 8. (a) XAS spectra taken at the $L_{2,3}$ edge of Mn with right (μ^+) and left (μ^-) circular polarization for **H**//**b** configuration at T=5 K and H=5 T. (b) Normalized XMCD spectra with 5 T magnetic field applied along the crystallographic **b** axis at T=5 K.

The XMCD spectrum at the Mn $L_{2,3}$ edges shows a negative signal at the L_3 edge and a very weak positive signal at the L_2 edge, which indicates that the Mn sublattice is polarized by the magnetic field at low temperatures and a small net magnetic moment contribution is induced within the proposed antiferromagnetic cycloidal configuration of the Mn moments in the *ab* plane[8]. The magnitude of the XMCD signal is much smaller (at least a factor 8) than the reported for the Tb $M_{4,5}$ edges (see fig. 2) and far from the expected ratio between the theoretical magnetic moments for fully saturated Mn^{3+} and Tb^{3+} sublattices. These results indicate that the small net magnetic moment of the Mn atoms along the applied field direction arises from a small canting of the antiferromagnetic Mn moments (cycloidal order). Moreover, the signs of the Mn and Tb XMCD signals are in agreement with a parallel alignment of the Mn and Tb sublattices and also parallel to the applied magnetic field, similar to other manganites.[35]

The field dependence of the Mn L_3 edge integrated XMCD signal normalized to the maximum of the corresponding averaged absorption spectra for **H**//**b** at T=5 K is shown in fig. 9. The Mn L_3 edge magnetometry curve increases continuously with increasing the magnetic field but the magnetic evolution does not follow the field dependence of the Tb-moments. Therefore, the different field dependence of the Mn and Tb sublattice magnetizations points towards the decoupling between Tb^{3+} and Mn^{3+} net moments under applied magnetic fields in agreement neutron diffraction measurements that report on a Tb

ferromagnetic ordering under applied magnetic fields (k=0) while Mn cycloidal antiferromagnetic ordering remains unaltered.[10,17]

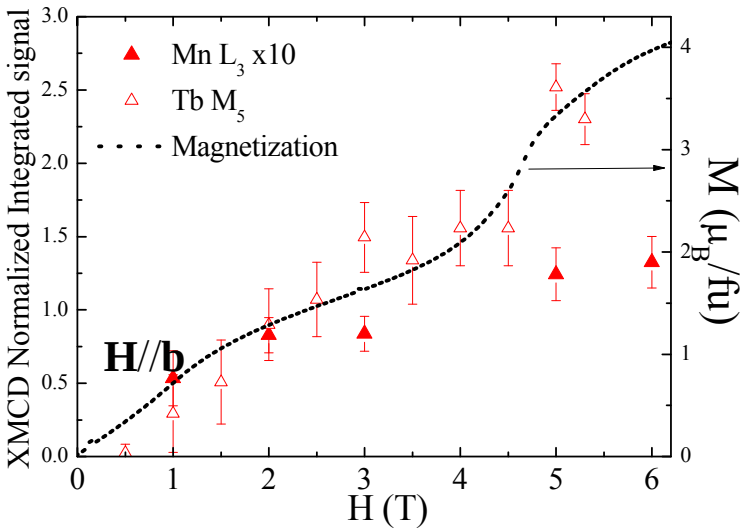

Figure 9. Normalized integrated XMCD intensity as a function of external field (taken at T=5 K) along the crystallographic *b* axis of the $TbMnO_3$ single crystal. Solid and open triangles refer to the Mn L_3 and the Tb M_5 integrated and normalized dichroic signals, respectively. Mn L_3 integrated signal is multiplied by 10 to be better visualized. Dashed line displays the reported magnetization measurement (right y-axis).

Finally, the temperature dependence of both the Mn and Tb sublattice magnetizations was measured at H=5 T in the temperature range from 5 K up to 100 K for this **H//b** configuration using TEY detection, as shown in fig. 10, compared to the magnetization M_b (intermediate behavior between the easy (**a**) and the hard (**c**) magnetization axes). The Tb M_5 integrated XMCD signal follows the same evolution with temperature as the macroscopic magnetization, indicating the main contribution of Tb magnetic moments to the bulk magnetization up to temperature values well above their ordering temperature $T_{N,Tb}$. The Mn L_3 integrated XMCD signal also shows a gradually decrease with increasing the temperature, which can be ascribed to the decreasing of the net magnetic moments of the Mn atoms on heating.

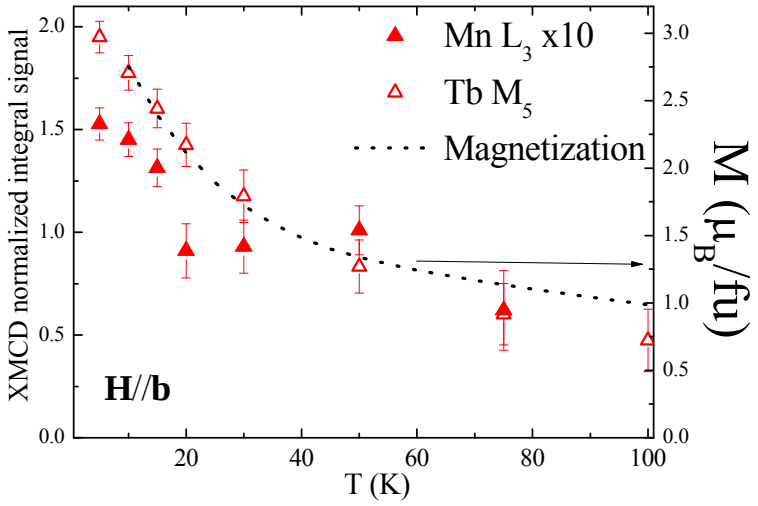

Figure 10. Macroscopic magnetization under a 5 T magnetic field along the **b** axis as a function of temperature (dotted line) compared with the Tb XMCD M_5 (open triangles) and Mn XMCD L_3 (solid triangles) integrated signals (multiplied by 10 for the sake of comparison) normalized to the maximum of their respective averaged absorption signals.

IV. Conclusions

The separated role of Tb and Mn sublattices on the magnetic properties of $TbMnO_3$ under applied magnetic fields have been studied by spectroscopic techniques sensitive to *f* and *d* states, respectively. At zero field, Tb and Mn magnetic orderings are coupled below T_{FE}=28 K[14], and are still correlated below T_N^{Tb},[9,13] differently from other manganites where RE= Dy, Ho[34]. Here, reflectivity and FY measurements of XMCD have been performed on $TbMnO_3$, and show that the amplitude of the dichroic signals at Tb $M_{4,5}$ edges reproduce the macroscopic magnetic anisotropy of $TbMnO_3$ as a function of the magnetic field at low temperatures (5 K). These results univocally demonstrate that Tb sublattice is the only responsible for the magnetic anisotropy in this compound. In addition, Tb magnetization never reaches saturation, so Tb is not simply magnetized along the field direction. This magnetic behavior is perfectly explained by considering the strong Ising character of the Tb^{3+} ions (J=6) and the low local symmetry of the nonequivalent Tb sites in the *Pbnm* structure. Therefore, Tb moments stay along their Ising axis within the *ab* plane. By contrast, the Mn-sublattice shows weak XMCD signals as a result of a small projection along the direction of the applied magnetic field along **b** axis. Besides that, the small Mn moment has been found to be parallel to the Tb moment, which confirms that Mn moments are canted following the applied field direction. This result proves the decoupling between the Tb and Mn magnetic sublattices by the application of an external magnetic field in agreement with previous neutron diffraction measurements[17], which lead to a noncollinear arrangement of the type C_xF_y (Bertaut's notation[37]) of the Tb moments together with a cycloid magnetic structure of the Mn moments in the *ab* plane when at least 5 T are applied along **b** direction.

Finally and according to the differentiated Tb and Mn sublattice contributions to the magnetic response in $TbMnO_3$ under applied magnetic fields, shown by this experimental

work, we discuss the role of the Tb^{3+} single ion anisotropy in the macroscopic magnetoelectrical response of this system. The observed strong crystalline anisotropy of Tb^{3+} forces Tb moments to be mostly confined along their Ising axes in the *ab* plane and only when applying H along those axes, the electric polarization is observed to be flopped from **c** to **a** axis for both **H**//**a** and **H**//**b** configurations. In both cases the new P orientation (P_a) is parallel to the Tb largest induced moment (m_a) component at high fields. Differently, the application of the magnetic field in the **c** direction does not induce any alignment of the Tb moments and thus the electrical polarization remains unaltered.[16] On the other hand, the oriented Mn magnetic moment along the field direction is very small so the cycloidal antiferromagnetic ordering of the Mn moments is poorly affected by an external magnetic field (figure 9).[17] Moreover, the magnetic coupling between Mn and Tb sublattices under applied magnetic fields is shown to be very subtle; consequently high fields are needed to flop one of the components of the Mn cycloid (and then P direction). Therefore, under applied magnetic fields magneto-crystalline coupling originated by Tb magnetic arrangement, instead of Mn^{3+} anisotropy as sometimes suggested in the literature[38,39], is proposed to play a significant role on the polarization flop from **c** to **a**. In other words, the Tb magnetic order (at $\mathbf{H_b}$=5T) should induce a motion of the oxygen atoms, which triggers a field-induced transition of the Mn moments into a configuration lying in the *ab* plane together with the flop of the polarization from the **c**-direction (zero field) to the **a**-direction (high-field). In summary, we show that the contribution from the Tb magnetic order to the electric polarization in $TbMnO_3$ cannot be ignored.

Acknowledgements

Authors are indebted to M. C. Sánchez for the orientation of the single crystals. Financial support from the Spanish MINECO (Project No. MAT2012-38213-C02-01 and MAT2011-23791) and the Diputación General de Aragón (CAMRADS) are acknowledged. We also thank the use of SAI from Universidad de Zaragoza and Bessy II synchrotron facility for beam time allocation and support during the experiments.

References

[1] Y. Tokura and S. Seki, Adv. Mater. **22**, 1554 (2010).
[2] Y. Tokura, Science **312**, 1481 (2006).
[3] M. Fiebig, J. Phys. D: Appl. Phys. **38**, R123 (2005).
[4] N. A. Hill, J. Phys. Chem. B **104** 6694, (2000).
[5] D. Khomskii, Physics **2** 20 (2009).
[6] I. A. Sergienko and E. Dagotto, Phys. Rev. B **73**, 094434 (2006).
[7] R. Kajimoto, H. Yoshizawa, H. Shintani, T. Kimura, and Y. Tokura, Phys. Rev. B **70**, 012401 (2004).
[8] M. Kenzelmann, A.B. Harris, S. Jonas, C. Broholm, J. Schefer, S.B. Kim, C.L. Zhang, S.-W. Cheong, O.P. Vajk and J.W. Lynn, Phys. Rev. Lett. **95** 087206, (2005)
[9] J. Voigt, J. Persson, J. W. Kim, G. Bihlmayer, and Th. Brückel., Phys. Rev. B **76** 104431 (2007).

[10] N. Aliouane, O. Prokhnenko, R. Feyerherm, M. Mostovoy, J. Strempfer, K. Habicht, K. C. Rule, E. Dudzik, A. U. B. Wolter, A. Maljuk and D. N. Argyriou, J. Phys.: Condens. Matter **20** 434215 (2008).
[11] D. Mannix, D. F. McMorrow, R. A. Ewings, A. T. Boothroyd, D. Prabhakaran, Y. Joly, B. Janousova, C. Mazzoli, L. Paolasini, and S. B.Wilkins, Phys. Rev. B **76** 184420 (2007).
[12] V. Cuartero, J. García, G. Subías, J. Herrero-Martín, J. Blasco and C. R. Natoli. J. Phys.: Conf. Series **430** 012101 (2013).
[13] O. Prokhnenko, R. Feyerherm, M. Mostovoy, N. Aliouane, E. Dudzik, A. U. B. Wolter, A. Maljuk, and D. N. Argyriou. Phys. Rev. Lett. **99**, 177206 (2007).
[14] S. B. Wilkins, T.R. Forrest, T.A.W. Beale, S.R. Bland, H.C. Walker, D. Mannix, F. Yakhou, D. Prabhakaran, A. T. Boothroyd, J. P. Hill, P. D. Hatton, and D.F. McMorrow. Phys. Rev. Lett. 103, 207602 (2009)
[15] T. Kimura, T. Goto, H. Shintani, K. Ishizka, T. Arima and Y. Tokura , Nature (London) **426,** 55 (2003).
[16] T. Kimura, G. Lawes, T. Goto, Y. Tokura, A. Ramirez. Phys. Rev. B **71**, 224425 (2005).
[17] V. Cuartero, J. Blasco, J. A. Rodríguez-Velamazán, J. García, G. Subías, C. Ritter, J. Stankiewicz and L. Canadillas-Delgado. Phys. Rev. B. **86,** 1044133 (2012).
[18] C.-C. Kao, C.T. Chen, E. D. Johnson, J. B. Hastings, H. J. Lin, G. H. Ho, G. Meigs, J.-M. Brot, S. L Hulbert, Y. U. Idzerda, C. Vettier. Phys. Rev. B **50**, 9599 (1994).
[19] J. Blasco, M. C. Sánchez, J. García, J. Stankiewicz, and J. Herrero-Martín, J. Cryst. Growth **310**, 3247 (2008).
[20] B. T. Thole, P. Carra, F. Sette, G. van der Laan. Phys. Rev. Lett. **68**, 1943 (1992).
[21] C. Bordel, S. Pizzini, J. Vogel, K. Mackay, J. Voiron, R. M. Galéra, A. Fontaine, P. Auric, J. B. Goedkoop and N. B. Brookes. Phys. Rev. B **56**, 8149 (1997).
[22] S. Stepanow, J. Honolka, P. Gambardella, L. Vitali, N. Abdurakhmanova, T.-C. Tseng, S. Rauschenbach, S. L. Tait, V. Sessi, S. Klyatskaya, M. Ruben and K. Kern. J. Am. Chem. Soc. **132**, 11900 (2010).
[23] R. Biagi, J. Fernandez-Rodriguez, M. Gonidec, A. Mirone, V. Corradini, F. Moro, V. de Renzi, U. del Pennino, J. C. Cezar, D. B. Amabilino and J. Veciana, Phys. Rev. B **82**, 224406 (2010).
[24] L. Tröger, D. Arvanitis, K. Baberschke, H. Michaelis, U. Grimm, and E. Zschech, Phys. Rev. B **46**, 3283 (1992).
[25] E. Stavitski and F. M. F. de Groot, *Micron* **41**, 687 (2010).
[26] P. H. Butler. *Point Group Symmetry Applications.* Springer (1981).
[27] Cowan, R. D. *The Theory of Atomic Structure and Spectra*; 365 University of California Press: Berkeley, CA (1981).
[28] P. Carra, B. T. Thole, M. Altarelli, X. Wang. Phys. Rev. Lett. **70**, 694 (1993).
[29] P. Carra, H. König, B. T. Thole, M. Altarelli. Phys. B **192**, 182 (1993).
[30] N. Abe, K. Taniguchi, S. Ohtani, T. Takenobu, Y. Iwasa, and T. Arima, Phys. Rev. Lett. **99**, 227206 (2007).
[31] J. Mareschal, J. Sivardière, G. F. De Vries and E. F. Bertaut, J. Appl. Phys. **39** 1364 (1968).
[32] S. Quezel F. Techeou, J. Rossat-Mignod, G. Quezel and E. Roudaut, Physica B&C **86-88**, 916 (1977).
[33] J. B. Gruber K. L. Nash, R. M. Yow, D. K. Sardar, U. V. Valiev, A. A. Uaokov, G. W. Burdick, J. Lumin. **128**, 1271 (2008).
[34] L. Holmes, R. Sherwood and L. G. Van Uitert, J. Appl. Physics **39**, 1373 (1968).
[35]M. Sikora, Cz. Kapusta, D. Zaja, W. Tokarz, K. Attenkofer, P. Fischer, E. Goering, G. Schütz, J. Alloys Comp. **328**, 100 (2001).

[36] J. Vogel M. Sacchi, R. J. H. Kappert, J. C. Fuggle, J. B. Goedkoop, N. Brookes, G. van der Laan, E. Marinero, J. Magn. Magn. Mater. **150**, 293 (1995).
[37] E. F. Bertaut, Acta Cryst. A24, 217 (1968).
[38] M. Mochizuki and N. Furukawa, Phys. Rev. B **80**, 134416 (2009)
[39] H. J. Xiang, S.-H. Wei, M.-H. Whangbo and J. L. F. Da Silva, Phys. Rev. Lett. **101**, 037209 (2008).